Is the Madden-Julian Oscillation a Moisture Mode?

Víctor C. Mayta[1*], Ángel F. Adames Corraliza[1]

[1]Department of Atmospheric and Oceanic Sciences, University of Wisconsin, Madison, Wisconsin

Key Points:

- The MJO satisfies the criteria to be defined as a moisture mode only over the eastern Indian Ocean (60-110°E).
- The unique climatological features of the Indian Ocean allow moisture modes to exist near the planetary scale.
- The MSE export in this basin is slow enough to allow for WTG balance and for moisture to govern convection evolution.

[*]Department of Atmospheric and Oceanic Sciences, University of Wisconsin, 1225 W Dayton St, Madison, WI 53706, USA.

Corresponding author: Victor C. Mayta, mayta@wisc.edu

Abstract

The governing thermodynamics of the Madden-Julian Oscillation (MJO) are examined using sounding and reanalysis data. On the basis of four objective criteria, results suggest that the MJO behaves like a moisture mode –a system whose thermodynamics is governed by moisture– only over the Indian Ocean. Over this basin, the small effective gross moist stability, i.e., a slow moist static energy (MSE) export by convection, and slow convective adjustment timescale allows moisture modes to exist for all zonal wavenumbers except 1. Elsewhere, the faster-propagating wavenumber 1-2 components are more prominent and the effective gross moist stability is higher, preventing weak temperature gradient (WTG) balance to be established and causing temperature and moisture to play similar roles in the MJO's thermodynamics.

Plain Language Summary

The Madden-Julian Oscillation is one of the most important phenomena that occur at the subseasonal to seasonal timescale and is a source of weather predictability at this timescale. In spite of its importance, many features of the MJO remain elusive and many theories have been proposed to understand its behavior. Arguably, the most well-known MJO theory is the moisture mode theory. The theory posits that moisture governs the evolution of the MJO. Here we show that this theory is applicable only over the Indian Ocean, where low atmospheric stability and long-lasting convection allow for moisture modes to exist. Elsewhere, temperature fluctuations in the MJO become as important as moisture, a feature that is inconsistent with moisture mode theory.

1 Introduction

The Madden-Julian oscillation (MJO) is the dominant and most well-known mode of intraseasonal variability over the tropics (Madden & Julian, 1971; Zhang, 2005). Its planetary-scale structure, intraseasonal time-scale, and slow eastward propagation at $\sim$5 m s^{-1} make this wave stand out from other forms of equatorial variability such as the equatorial waves (Kiladis et al., 2009). Recently, it has become clear that interactions between moisture, convection, radiation, and circulation are important for the dynamics of the MJO (Sobel et al., 2001; Raymond, 2001; Sobel & Maloney, 2013; Á. Adames & Kim, 2016; Gonzalez & Jiang, 2019; Á. Adames & Maloney, 2021; Ahmed, 2021; Wang & Sobel, 2021). These interactions can cause the dynamics of the MJO to significantly differ from those described by dry shallow water theory. Indeed, the MJO does not correspond to any of Matsuno's solutions (Matsuno, 1966).

Many theoretical models have been proposed to explain the MJO's features. These theories have been recently documented by Zhang et al. (2020) and Jiang et al. (2020). Among these theories, the moisture mode theory has arguably gained the most attention (Á. Adames & Maloney, 2021). In this theory, the evolution of moisture governs the evolution of the wave. The primary signatures of moisture modes are (a) a strong moisture tendency and (b) a weak temperature tendency (Á. Adames et al., 2019; Ahmed et al., 2021; Á. Adames & Maloney, 2021). The first condition manifests as a tight coupling between moisture and precipitation. The second condition ensures that the weak temperature gradient approximation (WTG; Sobel et al., 2001) is the dominant column energy balance. These two conditions underpin the criteria proposed in Mayta et al. (2022) to classify different tropical systems. By using these criteria, Mayta and Adames (2023) found that the MJO over the Western Hemisphere does not satisfy the conditions to be a moisture mode. Other studies have also argued that the circumnavigating MJO signature– where it is weakly coupled with convection– agrees with the convectively-coupled Kelvin wave rather than a moisture mode (Sobel & Kim, 2012; Powell, 2017; Á. Adames et al., 2019; Emanuel, 2020; Ahmed et al., 2021). However, other studies have shown that the

MJO's signature over the Indo-Pacific warm pool has the features of moisture modes (e.g., Myers & Waliser, 2003; Á. Adames & Kim, 2016; Kim et al., 2017; Á. Adames, 2017; Snide et al., 2022, ; among others).

These results give us the main scientific question of this study: Is the MJO a moisture mode? Is it possible that the MJO is a moisture mode only in some regions of the tropics? The structure of this paper is as follows: In section 2, we discuss the data and statistical methods used to explore moisture mode conditions associated with the MJO. In section 3, we examine the leading thermodynamic properties and assess its consistency with moisture mode theory (Á. Adames et al., 2019; Ahmed et al., 2021; Mayta et al., 2022). In section 4, we will employ a recent theory by Ahmed et al. (2021) to show that the MJO exhibits moisture mode behavior in regions where the atmosphere favors this behavior near the planetary scales. A concluding discussion is offered in section 5.

2 Data and Methods

2.1 Satellite CLAUS T_b and Reanalysis dataset

Satellite-observed brightness temperature (T_b) data is used in this study as a proxy for convection. The satellite data is obtained from the Cloud Archive User System (CLAUS) (Hodges et al., 2000). Three-dimensional (27 pressure levels) fields from the European Centre for Medium-Range Weather Forecasts ERA-5 reanalysis (ERA5; Hersbach et al., 2019) are used to explore moist thermodynamics associated with the MJO. The ERA5 dataset uses a 1.0° horizontal resolution grid, with four times daily analyses that match the CLAUS T_b data for the 36-yr time period 1984 through 2015. We make use of the zonal (u), meridional (v), and vertical winds (ω), specific humidity (q), temperature (T), diabatic heating rate (Q_1), surface and top of the atmosphere radiative fluxes, surface sensible and latent heat fluxes (SH and LE, respectively), and precipitation (P).

2.2 Field campaign data

To further analyze the moist process in the MJO and verify the accuracy of reanalysis data, we used observed data from three field campaigns around the tropical belt: (i) Over the Indian Ocean, we use data from the Dynamics of the Madden-Julian Oscillation (DYNAMO) field campaign, conducted from October 2011 through March 2012 (Yoneyama et al., 2013). We used data from the northern sounding array (NSA) averages from observations, located in the central equatorial Indian Ocean for a 3-month period from 10 October through 31 December 2011. The sounding array dataset was quality-controlled and bias corrected to create a DYNAMO legacy dataset (Ciesielski et al., 2014). (ii) In the Western Pacific, we used data collected during intensive operating period (IOP) of TOGA-COARE for a 4-month period from 1 November through 28 February 1993. A detailed description of sounding stations and quality control procedures for TOGA-COARE was documented in Webster and Lukas (1992). All calculations we present are average vertical profiles for grid points within Intensive Flux Array (IFA), which is an array of sounding stations centered near 2°S,155°E (Fig. 1). (iii) For tropical South America, the Observations and Modeling of the Green Ocean Amazon (GoAmazon 2014/15) are used. The field campaign was carried out in central Amazonia, Brazil for a two-year time period from 1 January 2014 through 31 December 2015. For this study, we make use of the constrained variational analysis product for GoAmazon (VARANAL; Tang et al., 2016). VARANAL is derived from the ECMWF analysis fields and Atmospheric Radiation Measurement's (ARM) observations during GoAmazon 2014/15 using the constrained variational analysis proposed in Zhang and Hendon (1997). This product assimilates the top of the atmosphere and surface observations to produce thermodynamic budgets. The surface observations assimilated include surface radiative, latent, and sensible heat fluxes and precipitation from the System for the Protection of Amazonia (SIPAM)

radar. Additional details about VARANAL products during GoAmazon 2014/15 are found in Tang et al. (2016).

Finally, we make use of the all-season OLR MJO index (OMI; Kiladis et al., 2014) as a measure of MJO activity. This index represents the circulation and convection MJO features and is commonly used to track the life cycle of an MJO event.

2.3 Linear regression

Thermodynamic anomaly fields associated with the MJO are obtained by projecting raw ERA5 data at each grid point onto the associated first principal component (OMI1) time series. Then, all fields are scaled to one standard deviation OMI1 perturbation as made in previous studies (e.g., Mapes et al., 2006; Á. Adames et al., 2021; Snide et al., 2022; Mayta et al., 2022). The same approach is applied to data from campaigns. The area-average of filtered T_b or data at the same grid base point of the observations is used to calculate regressions instead. The statistical significance of these results is then assessed based on the two-tailed Student's t-test. This method takes into account the correlation coefficients and an effective number of independent samples (degrees of freedom) based on the decorrelation timescale (Livezey & Chen, 1983).

3 Moist Thermodynamics of the MJO

We will now examine three criteria first described by Ahmed et al. (2021), applied to the entire tropical belt. In Mayta et al. (2022), these criteria were modified to make them more suitable for their diagnosis in observational and reanalysis data. These criteria are:

(a) **Criterion 1 (C1): The wave must exhibit a large moisture signature that is highly correlated with the precipitation anomalies**
For the MJO to be considered a moisture mode, its signature in column water vapor ($\langle q \rangle'$) must be large enough to explain the majority of the surface rainfall variance (P'), given the following relation,

$$P' \propto \langle q \rangle' \tag{1}$$

This results in a strong correlation ($\sim$0.9 rounded) between P' and $\langle q \rangle'$ (Mayta et al., 2022; Mayta & Adames, 2023). In this study, $\langle \cdot \rangle \equiv 1/g \int_{surf.}^{top} (\cdot) dp$ denotes the mass-weighted vertical integral and primes ($'$) represent intraseasonal anomalies.
We apply this criterion by constructing a scatterplot between P' and $\langle q \rangle'$ at each grid point in the reanalysis (Fig. 1a) and at the corresponding base point for the field campaign data (Fig. 2). The correlations between P' and $\langle q \rangle'$ from ERA5 are plotted in Fig. 1a, and the latitudinal averages in Fig. 1d. Results show that only over the Indo-Pacific warm pool region passes the first criterion, with correlations ranging close to $\sim$1.0. An exception occurs in the Maritime Continent, where correlations are beneath 0.9. Correlations decay drastically outside of the warm pool, from 150°W to 40°E, where the mean correlation value is of $\sim$0.5 (Fig. 1d).
When data from the field campaigns are analyzed instead, we see that a strong correlation between P' and $\langle q \rangle'$ is seen for the DYNAMO data (Fig. 2a). As the MJO moves away from the warm pool, correlations decrease as depicted in the TOGA-COARE data, where a correlation between P' and $\langle q \rangle'$ is about $\sim$0.75 (Fig. 2d). The cyclical appearance of the cloud of points is suggestive of a lead/lag relationship between the two fields, rather than an in-phase one. A high correlation of $\sim$0.98 (Fig. 2h) is seen once again at the GoAmazon base point, in disagreement with ERA5.

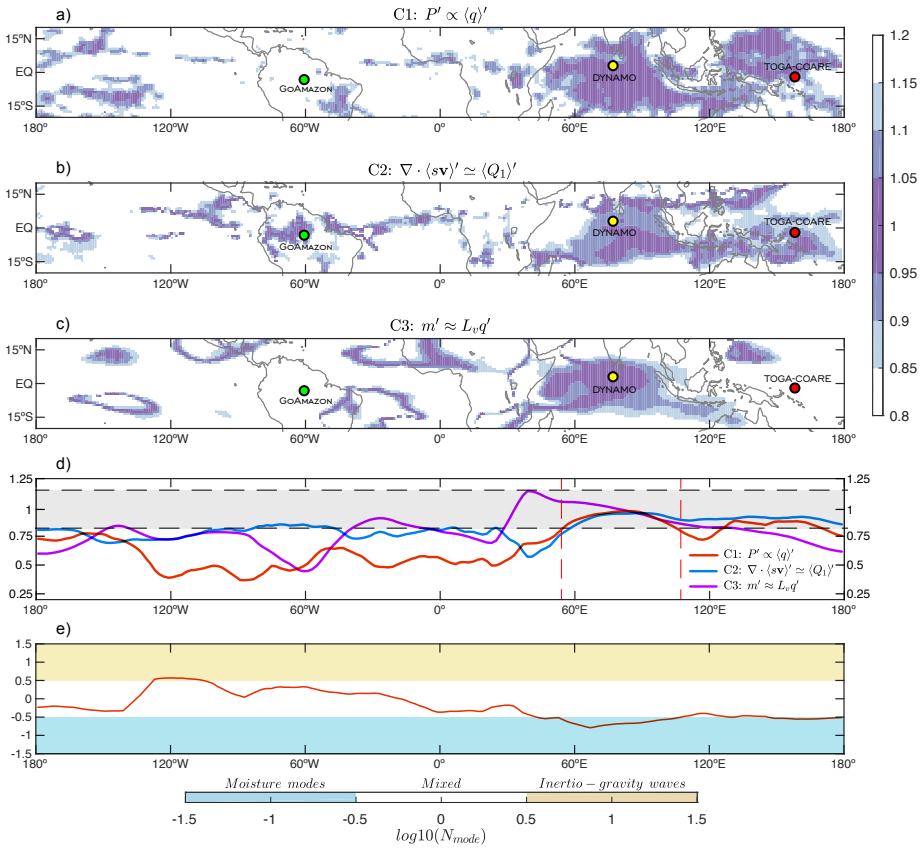

Figure 1. Geographical variations of the moisture mode criteria. Maps of (a) P′ vs $\langle q \rangle'$, (b) $\nabla \cdot \langle s\mathbf{v} \rangle'$ vs $\langle Q_1 \rangle'$, and (c) $\langle m \rangle'$ vs $\langle L_v q \rangle'$. Anomalies are obtained by projecting ERA5 data at each grid point onto the associated first principal component (OMI1) time series. Panel (a) shows the correlation coefficient, and panels (b) and (c) are the slopes of the linear fitting. (d) Represents the average value of each criterion computed from 10°S to 10°N at each longitude. The gray shading represents the threshold (0.85 to 1.1) necessary to satisfy the moisture mode criteria. The red dashed lines indicate the longitude domain where the three criteria are satisfied. Panel (e) shows the geographical variation of the dimensionless N_{mode} parameter. Shadings represent base 10 logarithm of N_{mode}, where blue represents N_{mode} values categorized as moisture modes, yellow can be considered inertio-gravity waves, and white represents mixed systems. The location of the DYNAMO, TOGA-COARE, and GO-Amazon sites is indicated by a yellow, red, and green circle, respectively.

(b) **Criterion 2 (C2): The mode must be in weak temperature gradient (WTG) balance**

WTG balance is the leading thermodynamic balance in the tropics (Sobel et al., 2001). This balance states that vertical dry static energy (DSE) advection approximately balances heating

$$\nabla \cdot \langle s\mathbf{v} \rangle' \simeq \langle Q_1 \rangle' \tag{2}$$

where $s = C_p T + \phi$ is DSE, $\mathbf{v} = u\mathbf{i} + v\mathbf{j}$ is the horizontal vector wind field, $C_p = 1004$ is the specific heat at constant pressure, and T is the temperature. $\langle Q_1 \rangle' \simeq \langle Q_r \rangle' + L_v P' + SH'$ is the apparent heating rate and can be calculated from reanalysis and observations following Yanai and Johnson (1993), where Q_r

is the radiative heating rate, SH is the surface sensible heat flux, and L_v represents the latent heat of vaporization (2.5×10^6 J kg $^{-1}$). To pass this criterion, the MJO must exhibit a slope of the linear least-square fit within the margin of ∼0.9-1.1 (rounded).

Fig. 1b shows the value of the slope of the linear least-square fit at each grid point. We can see that the slope is ∼1 from the Indian Ocean towards the Western Pacific. Regions over the mean climatological ITCZ position, including the Amazon basin, are also places where this criterion is satisfied. The meridionally-averaged values (Fig. 1d) show that the criterion largely prevails from 50°E to 180°. Observations are also in agreement with reanalysis. Results show a high correlation between $\nabla \cdot \langle s\mathbf{v} \rangle'$ and $\langle Q_1 \rangle'$, with a slope of ∼0.99, ∼0.97, and ∼0.99 for DYNAMO, TOGA-COARE, and GoAmazon, respectively (Figs. 2b, e, i).

(c) **Criterion 3 (C3): Moisture must govern the distribution of moist static energy (MSE)**

If the MJO is a moisture mode, moisture should be the main contributor to MSE, implying that

$$\langle m \rangle' \approx L_v \langle q \rangle' \tag{3}$$

where $m = s + L_v q$ is MSE. As in C2, a slope of the linear least-square fit within the margin of ∼0.9-1.1 (rounded) is needed to guarantee the balance of Eq. (3). From Fig. 1c, we see that the slope of the linear fit is ∼1 only over the Indian Ocean. According to the average values presented in Fig. 1d (solid magenta line), this criterion is satisfied from 45°E to 130°E. Results from ERA5 can be verified with observations at different base points. From DYNAMO (Fig. 2c) it is possible to see that the slope is about ∼1 over the Indian Ocean. The slope diminishes at the TOGA-COARE base point (0.88, Fig. 2f), and completely falls outside the threshold over GoAmazon (1.66, Fig. 2i).

(d) N_{mode}

In addition to the three aforementioned criteria, we can also estimate the value of N_{mode}, which can be computed as in Á. Adames et al. (2019),

$$\mathrm{N}_{mode} \simeq \frac{c_p^2 \tau}{c^2 \tau_c} \tag{4}$$

where c is the phase speed of a first baroclinic free gravity wave ($c \simeq 50\ ms^{-1}$), c_p is the phase speed of the MJO, τ_c is the convective moisture adjustment time scale, and τ is the temporal time scale. When $\mathrm{N}_{mode} \ll 1$, moisture governs the thermodynamics of the MJO, resulting in moisture modes; but if $\mathrm{N}_{mode} \gg 1$ the thermodynamics of a wave are predominantly driven by thermal fluctuations, resulting in gravity waves. When $\mathrm{N}_{mode} \approx 1$ the MJO will exhibit the behavior of both moisture mode and gravity wave.

Figure 1e shows the geographical variation of the base 10 logarithm of the dimensionless N_{mode} parameter. From Eq. (4), τ_c varies at each longitude (Fig. S1a), τ is assumed to be 45 days, the average value throughout the tropics and c_p is computed for different regions (see Table S1). The zonal distribution of N_{mode} is in qualitative agreement with the three criteria discussed above. Values of N_{mode} smaller than 0.3 are observed exclusively from 60°E throughout 180°. The smallest value of N_{mode} is found over the Eastern Indian Ocean (60°E–90°E, Fig. 1e), where the MJO propagates slowly at about ∼4.1 m s^{-1} (Table S1). In contrast, larger values of N_{mode} are observed over the Eastern Pacific, in a region where the wave propagates faster.

When all conditions are examined together, we conclude that the MJO is a moisture mode only over the eastern Indian Ocean (60°E to 110°E; Fig. 1d). Elsewhere, it is not a moisture mode but rather a so-called quasi-equilibrium mode (Ahmed et al., 2021)

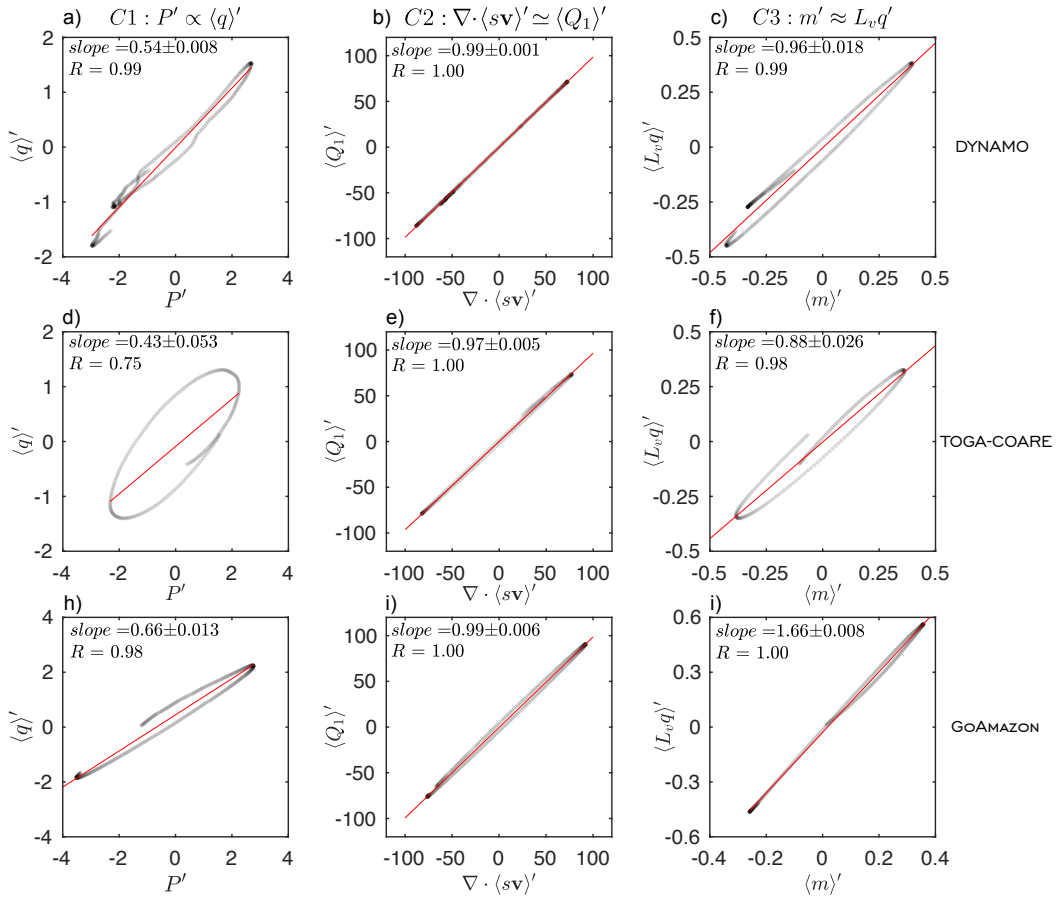

Figure 2. Scatterplots of P′ vs $\langle q \rangle'$ (first column), $\nabla \cdot \langle s\mathbf{v} \rangle'$ vs $\langle Q_1 \rangle'$ (second column), and $\langle m' \rangle$ vs $\langle L_v q' \rangle$ (third column) for the DYNAMO (top panels), TOGA-COARE (middle panels), and GoAmazon (bottom panels), respectively. Anomalies are obtained by regressing all fields against the time series of the filtered T_b at the corresponding base point of the field campaign (See Fig. 1). The linear least squares fit is shown as a solid red line. The slope of the linear fit and the correlation coefficient are shown in the top-left of each panel.

or a mixed-moisture gravity wave (Á. Adames et al., 2019; Á. F. Adames, 2022), as will be discussed in the following section.

In order to objectively quantify the regional dependence of the moisture mode features of the MJO, the seasonal (Nov-Apr) space-time spectra of T_b for two different sectors of the tropics is shown in Figure 3: Indo-Pacific (10°N–10°S, 60°E–180°) and Eastern Pacific - Atlantic (10°N–10°S, 120°W–0°). More details about the calculation of regional spectra can be found in the figure caption. The wavenumber-frequency distribution of base 10 logarithms of N_{mode}, following a similar procedure of Á. F. Adames (2022), is also depicted as shading. Areas shaded in blue are moisture modes. Each spectrum shows clear evidence of the differences in the intraseasonal time scale (periods more than 20 days). In the Indo-Pacific spectrum (Fig. 3a), a wide range of zonal wavenumbers ($k \approx 0-7$). The peaks are centered at wavenumbers $k = 2-3$, in a region where moisture modes are expected according to the N_{mode} spectrum. However, the story is quite different in the Eastern Pacific and Atlantic spectrum (Fig. 3b), where stronger power spectra are mainly concentrated in planetary wavenumbers $k \approx 1-2$ and frequencies of

~20-50 days. According to the N_{mode} wavenumber-frequency spectra, the intraseasonal signal over these regions is clearly located in the mixed moisture-gravity wave regime (Á. F. Adames, 2022).

4 The Moisture Mode Cutoff Wavenumber (k_{moist})

Table 1. Table of constants used in this study with their units and values. The calculation was conducted considering two separate regions, over and outside the warm pool region.

Parameter	Description	Value		Units
		Indo-Pacific	E. Pacific-Atlantic	
c	Dry gravity wave speed	50	50	m s^{-1}
m_{eff}	Effective gross moist stability	0.05	0.28	–
τ_q	Moisture sensitivity	27.2	13	h
τ_t	Temperature sensitivity	16.1	9.7	h
r	Cloud-radiative feedback parameter	0.13	0.07	–

In order to better understand the differences in the spectral signal shown in Fig. 3, we will employ the linear theory of Ahmed et al. (2021) to assess whether the different behavior is a result of mean state differences. Their theory examined the dispersion relation of an MJO-like mode without assuming moisture mode a-priory. They found the existence of a "moisture mode cutoff wavenumber" (k_{moist}), which describes the wavenumber in which longwave quasi-equilibrium (QE) modes (or mixed moisture-gravity waves) transition to WTG moisture modes. According to Ahmed et al. (2021) moisture modes exist when $k > k_{moist}$. The value of k_{moist}, is determined from the following relation,

$$k_{moist} \approx \frac{2}{c}\sqrt{\frac{m_{eff}(\tau_t + \tau_q)}{\tau_q^2 \tau_t}} \tag{5}$$

where m_{eff} is the effective gross moist stability (GMS), defined as a measure of the GMS that includes the impact of the radiative heating in the export of MSE (e.g., Inoue et al., 2020). The terms τ_t and τ_q are the sensitivity of convection to temperature and moisture fluctuations, respectively. A detailed derivation and scale analysis of Eq. (5) is explained in the supplementary material. The values of τ_t and τ_q in Eq. (5) are estimated as in Ahmed et al. (2020), where precipitation can be related to moisture and temperature by using a multiple linear regression model as follows,

$$P' = \frac{\langle q \rangle'}{\tau_q} - \frac{C_p}{L_v}\frac{\langle T \rangle'}{\tau_t} \tag{6}$$

By using Eq. (6), we obtain the values of the convective sensitivities τ_t and τ_q for the warm pool region of about 16.1 and 27.2 hours (Table 1), respectively. These values are longer than those used in Ahmed (2021). Outside the warm pool, the values of τ_t and τ_q decrease to 9.7 and 13.0 hours, respectively. Thus, the cooler tropospheric temperature outside the warm pool quantitatively impacts the convection moisture sensitivity (Ahmed et al., 2020). In addition, considering that the moisture mode cutoff wavenumber depends on m_{eff} (Ahmed et al., 2021), we also computed the value of m_{eff} from reanalysis for two distinct regions over the tropics. For the MJO, we found a value of

$m_{eff} \sim 0.05$ over the Indo-Pacific warm pool region (Fig. S2c and Table 1). In contrast, the value of m_{eff} is larger outside of the warm pool ($m_{eff} \sim 0.28$), causing k_{moist} to be larger.

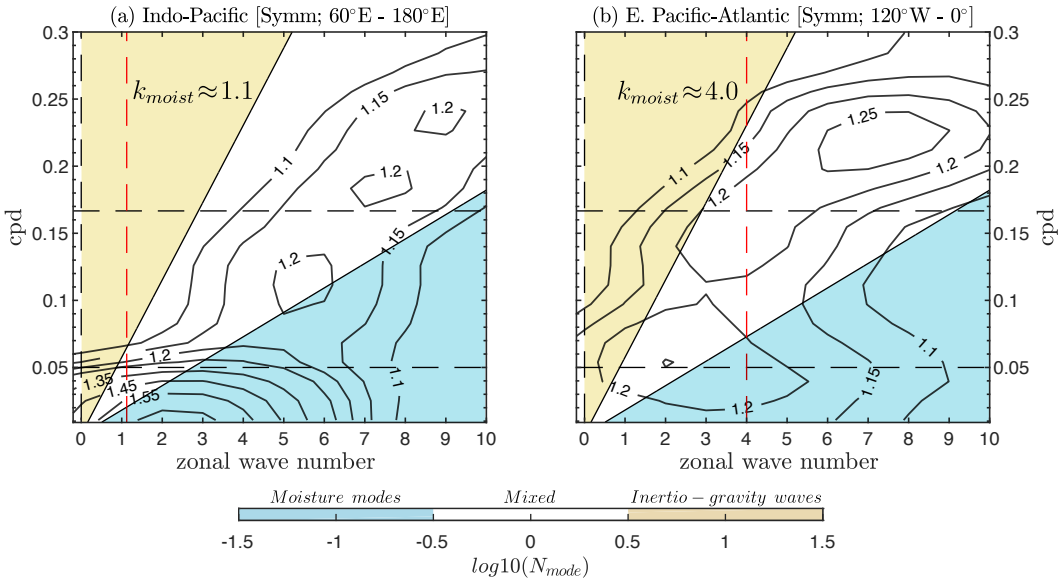

Figure 3. Regional wavenumber-frequency power spectrum (contours) of the symmetric component of CLAUS T_b calculated for (a) Indo-Pacific [10°N–10°S, 60°E–180°E] and (b) Eastern Pacific - Atlantic [10°N–10°S, 120°W–0°] and for the extended boreal winter (November-April). The functional form of the tapering window is the same as described in Wheeler and Kiladis (1999). Background spectra were estimated separately for the regional domain, using the smoothing procedure of Dias and Kiladis (2014). Contour interval is 0.05. Shadings represent wavenumber-frequency distribution of base 10 logarithm of N_{mode} following similar procedure of Á. F. Adames (2022). Blue shading represents tropical systems that can be categorized as moisture modes, yellow can be considered inertio-gravity waves, and white represents mixed systems. The red dashed lines in both panels indicate the moisture mode cutoff wavenumber (k_{moist}).

Replacing all these values into Eq. (5), we obtain a value of $k_{moist} \approx 1.1$ for the warm pool region and $k_{moist} \approx 4.0$ elsewhere (dashed red lines in Fig. 3). That $k_{moist} \approx 1.1$ over the warm pool means that moisture modes can extend to the planetary length scale (except for $k = 1$) since to m_{eff} is nearly to zero. Spectral peaks are observed at wavenumbers $k = 2-3$ (Fig. 3a), indicating that the peak MJO signal is expected to behave as a moisture mode in this region, consistent with the N_{mode} analysis. In contrast, outside the warm pool region (Fig. 3b) $k_{moist} \approx 4.0$ because of the larger effective GMS ($m_{eff} \approx 0.28$). Over the Eastern Pacific-Atlantic region, the signal strength is mainly concentrated in planetary wavenumbers $k \approx 1-3$. The strongest MJO signal in this region is concentrated over the mixed gravity wave spectrum (white shading in Fig 3). Thus the result of the k_{moist} analysis is largely consistent with the results of the four criteria discussed in the previous section.

5 Summary and conclusions

On basis of four criteria to identify moisture modes proposed in previous works (Á. Adames et al., 2019; Ahmed et al., 2021; Mayta et al., 2022), we demonstrated that the MJO can

be considered a moisture mode only over the Indian Ocean (60°E to 110°E; Fig. 1d). Elsewhere, the MJO has properties of both moisture mode and gravity wave. By using the theory proposed by Ahmed et al. (2021), we found that two factors explain why the MJO behaves like a moisture mode over the Indian Ocean: (i) a small effective gross moist stability ($m_{eff} \to 0$); and (ii) a slow convective adjustment timescale. These two features allow moisture modes to exist at the largest zonal scales in this region (except wavenumber 1; Fig. 3a).

The opposite occurs outside the Indian Ocean; most of the MJO signal is observed in wavenumbers $k \sim 1{-}2$, falling in the mixed moisture-gravity wave part of the N_{mode} spectrum (Fig. 3b). Over this region, the effective gross moist stability is almost five times larger than over the warm pool ($m_{eff} \approx 0.28$) and the convective adjustment timescale is faster. Under these conditions, WTG balance is not achieved at the MJO scale and temperature and moisture fluctuations play comparable roles. These results are in agreement with previous works that posited that the planetary-scale component of the MJO is not a moisture mode (Powell, 2017; Á. Adames et al., 2019; Ahmed et al., 2021; Chen, 2022; Mayta & Adames, 2023). In other words, the circumnavigating MJO component outside of the warm pool exhibits features that are more akin to a Kelvin wave (e.g., Sobel & Kim, 2012).

The results of this study have several implications. First, more theoretical work must be done to understand how a zonally-varying mean state affects the MJO. These results could also help us understand the scale selection mechanism of the MJO, which is likely not determined by moisture mode processes. Furthermore, the transition from moisture mode to a mixed wave should be examined further, especially with more GCMs. While not discussed here, this transition may help us further understand the Maritime Continent barrier effect (Zhang & Ling, 2017), and the MJO-QBO connection (Son et al., 2017), both of which occur in the region where the MJO begins to exhibit a transition from a moisture mode to a mixed mode. Lastly, it is curious that MJO initiation occurs in the region where moisture mode behavior is observed. It is possible that deviations from WTG balance play an important role in exciting moisture modes, as Snide et al. (2022) posited. All of these outstanding questions may be fruitful directions for future research.

6 Open Research

The dataset used in this study are available at ECWF (ERA5; `https://doi.org/10.24381/cds.adbb2d47`), the Atmospheric Radiation Measurement (ARM) program archive (VARANAL; `https://iop.archive.arm.gov/arm-iop/0eval-data/xie/scm-forcing/iop_at_mao/GOAMAZON/2014-2015/`) [registration is required to access data], TOGA-COARE dataset are available at `https://data.eol.ucar.edu/dataset/dsproj?TOGA_COARE`, and the interpolated CLAUS T_b data is available at `https://catalogue.ceda.ac.uk/uuid/ce476101711ce73107c9e90265ec6d9a`. DYNAMO NSA array averages from observations data (Version 3a) are available at `http://johnson.atmos.colostate.edu/dynamo/`. The OMI index is available at `https://psl.noaa.gov/mjo/mjoindex/`.

Acknowledgments

VM and ÁFAC are supported by NOAA grant number NA22OAR4310611. VM and ÁFAC was also supported by NSF CAREER grant number 2236433 and by the University of Wisconsin startup package. The contents of the manuscript were significantly improved after conversations with Fiaz Ahmed.

References

Adames, Á. (2017). Precipitation Budget of the Madden–Julian Oscillation. *Journal of the Atmospheric Sciences*, *74*(6), 1799 - 1817. doi: 10.1175/JAS-D-16-0242.1

Adames, Á., & Kim, D. (2016). The MJO as a Dispersive, Convectively Coupled Moisture Wave: Theory and Observations. *Journal of the Atmospheric Sciences*, *73*(3), 913 - 941. doi: 10.1175/JAS-D-15-0170.1

Adames, Á., Kim, D., Clark, S. K., Ming, Y., & Inoue, K. (2019). Scale Analysis of Moist Thermodynamics in a Simple Model and the Relationship between Moisture Modes and Gravity Waves. *Journal of the Atmospheric Sciences*, *76*(12), 3863 - 3881. doi: 10.1175/JAS-D-19-0121.1

Adames, Á., & Maloney, E. D. (2021). Moisture Mode Theory's Contribution to Advances in our Understanding of the Madden-Julian Oscillation and Other Tropical Disturbances. *Current Climate Change Reports*. doi: 10.1007/s40641-021-00172-4

Adames, Á., Powell, S. W., Ahmed, F., Mayta, V. C., & Neelin, J. D. (2021). Tropical Precipitation Evolution in a Buoyancy-Budget Framework. *Journal of the Atmospheric Sciences*, *78*(2), 509 - 528. doi: 10.1175/JAS-D-20-0074.1

Adames, Á. F. (2022). The Basic Equations Under Weak Temperature Gradient Balance: Formulation, Scaling, and Types of Convectively-coupled Motions. *Journal of the Atmospheric Sciences*, *79*(8), 2087 - 2108. doi: 10.1175/JAS-D-21-0215.1

Ahmed, F. (2021). The MJO on the Equatorial Beta Plane: An Eastward-Propagating Rossby Wave Induced by Meridional Moisture Advection. *Journal of the Atmospheric Sciences*, *78*(10), 3115 - 3135. doi: 10.1175/JAS-D-21-0071.1

Ahmed, F., Adames, Á. F., & Neelin, J. D. (2020). Deep Convective Adjustment of Temperature and Moisture. *Journal of the Atmospheric Sciences*, *77*(6), 2163-2186. doi: 10.1175/JAS-D-19-0227.1

Ahmed, F., Neelin, J. D., & Adames, Á. F. (2021). Quasi-equilibrium and weak temperature gradient balances in an equatorial beta-plane model. *Journal of the Atmospheric Sciences*, *78*(1), 209 - 227. doi: 10.1175/JAS-D-20-0184.1

Chen, G. (2022). The Amplification of Madden–Julian Oscillation Boosted by Temperature Feedback. *Journal of the Atmospheric Sciences*, *79*(1), 51 - 72. doi: 10.1175/JAS-D-21-0146.1

Ciesielski, P. E., Yu, H., Johnson, R. H., Yoneyama, K., Katsumata, M., Long, C. N., ... Hove, T. V. (2014). Quality-controlled upper-air sounding dataset for dynamo/cindy/amie: Development and corrections. *Journal of Atmospheric and Oceanic Technology*, *31*(4), 741-764.

Dias, J., & Kiladis, G. N. (2014). Influence of the basic state zonal flow on convectively coupled equatorial waves. *Geophysical Research Letters*, *41*(19), 6904–6913. Retrieved from `http://dx.doi.org/10.1002/2014GL061476` doi: 10.1002/2014GL061476

Emanuel, K. (2020). Slow modes of the equatorial waveguide. *Journal of the Atmospheric Sciences*, *77*(5), 1575–1582.

Gonzalez, A. O., & Jiang, X. (2019). Distinct propagation characteristics of intraseasonal variability over the tropical west pacific. *Journal of Geophysical Research: Atmospheres*, *124*(10), 5332-5351. doi: https://doi.org/10.1029/2018JD029884

Hersbach, H., Bell, W., Berrisford, P., Horányi, A., J., M.-S., Nicolas, J., ... Dee, D. (2019). Global reanalysis: goodbye ERA-Interim, hello ERA5. , 17-24. doi: 10.21957/vf291hehd7

Hodges, K. I., Chappell, D. W., Robinson, G. J., & Yang, G. (2000). An improved algorithm for generating global window brightness temperatures from multiple

satellite infrared imagery. *Journal of Atmospheric and Oceanic Technology*, *17*(10), 1296–1312.

Inoue, K., Adames, Á. F., & Yasunaga, K. (2020). Vertical Velocity Profiles in Convectively Coupled Equatorial Waves and MJO: New Diagnoses of Vertical Velocity Profiles in the Wavenumber-Frequency Domain. *Journal of the Atmospheric Sciences*, *77*(6), 2139 - 2162. doi: 10.1175/JAS-D-19-0209.1

Jiang, X., Adames, F., Kim, D., Maloney, E. D., Lin, H., Kim, H., ... Klingaman, N. P. (2020). Fifty Years of Research on the Madden-Julian Oscillation: Recent Progress, Challenges, and Perspectives. *Journal of Geophysical Research: Atmospheres*, *125*(17), e2019JD030911. doi: https://doi.org/10.1029/2019JD030911

Kiladis, G. N., Dias, J., Straub, K. H., Wheeler, M. C., Tulich, S. N., Kikuchi, K., ... Ventrice, M. J. (2014). A Comparison of OLR and Circulation-Based Indices for Tracking the MJO. *Monthly Weather Review*, *142*(5), 1697 - 1715. doi: 10.1175/MWR-D-13-00301.1

Kiladis, G. N., Wheeler, M. C., Haertel, P. T., Straub, K. H., & Roundy, P. E. (2009). Convectively coupled equatorial waves. *Reviews of Geophysics*, *47*(2).

Kim, D., Kim, H., & Lee, M.-I. (2017). Why does the MJO detour the Maritime Continent during austral summer? *Geophysical Research Letters*, *44*(5), 2579-2587. doi: 10.1002/2017GL072643

Livezey, R. E., & Chen, W. Y. (1983). Statistical field significance and its determination by Monte Carlo techniques. *Mon. Wea. Rev.*, *111*, 46-59.

Madden, R. A., & Julian, P. R. (1971). Detection of a 40-50-day oscillation in the zonal wind in the tropical Pacific. *J. Atmos. Sci.*, *29*, 1109–1123.

Mapes, B., Tulich, S., Lin, J., & Zuidema, P. (2006). The mesoscale convection life cycle: Building block or prototype for large-scale tropical waves? *Dynamics of Atmospheres and Oceans*, *42*(1), 3 - 29. doi: https://doi.org/10.1016/j.dynatmoce.2006.03.003

Matsuno, T. (1966). Quasi-geostrophic motions in the equatorial area. *Journal of the Meteorological Society of Japan*, *44*, 25–43.

Mayta, V. C., & Adames, A. F. (2023). Moist Thermodynamics of Convectively Coupled Waves over the Western Hemisphere. *Journal of Climate*, 1–36. doi: 10.1175/JCLI-D-22-0435.1

Mayta, V. C., Adames, Á. F., & Ahmed, F. (2022). Westward-propagating Moisture Mode over the Tropical Western Hemisphere. *Geophysical Research Letters*, e2022GL097799.

Myers, D. S., & Waliser, D. E. (2003, 2014/12/30). Three-Dimensional Water Vapor and Cloud Variations Associated with the Madden–Julian Oscillation during Northern Hemisphere Winter. *J. Climate*, *16*(6), 929–950.

Powell, S. W. (2017). Successive MJO propagation in MERRA-2 reanalysis. *Geophysical Research Letters*, *44*(10), 5178-5186. doi: https://doi.org/10.1002/2017GL073399

Raymond, D. J. (2001). A New Model of the Madden–Julian Oscillation. *Journal of the Atmospheric Sciences*, *58*(18), 2807 - 2819. doi: 10.1175/1520-0469(2001)058⟨2807:ANMOTM⟩2.0.CO;2

Snide, C. E., Ángel F. Adames, Powell, S. W., & Mayta, V. C. (2022). The Role of Large-Scale Moistening by Adiabatic Lifting in the Madden–Julian Oscillation Convective Onset. *Journal of Climate*, *35*(1), 269 - 284. doi: 10.1175/JCLI-D-21-0322.1

Sobel, A., & Kim, D. (2012). The MJO-Kelvin wave transition. *Geophysical Research Letters*, *39*(20), 1-5. doi: https://doi.org/10.1029/2012GL053380

Sobel, A., & Maloney, E. (2013). Moisture modes and the eastward propagation of the mjo. *Journal of the Atmospheric Sciences*, *70*(1), 187 - 192. doi: 10.1175/JAS-D-12-0189.1

Sobel, A., Nilsson, J., & Polvani, L. M. (2001). The weak temperature gradient

approximation and balanced tropical moisture waves. *Journal of the Atmospheric Sciences*, *58*(23), 3650 - 3665. doi: 10.1175/1520-0469(2001)058⟨3650:TWTGAA⟩2.0.CO;2

Son, S.-W., Lim, Y., Yoo, C., Hendon, H. H., & Kim, J. (2017). Stratospheric control of the madden–julian oscillation. *Journal of Climate*, *30*(6), 1909–1922.

Tang, S., Xie, S., Zhang, Y., Zhang, M., Schumacher, C., Upton, H., ... Thieman, M. (2016). Large-scale vertical velocity, diabatic heating and drying profiles associated with seasonal and diurnal variations of convective systems observed in the GoAmazon2014/5 experiment. *Atmos. Chem. Phys.*, *16*(22), 14249–14264. doi: 10.5194/acp-16-14249-2016

Wang, S., & Sobel, A. H. (2021). A unified moisture mode theory for the madden julian oscillation and the boreal summer intraseasonal oscillation. *Journal of Climate*, 1–71.

Webster, P. J., & Lukas, R. (1992). TOGA COARE: The Coupled Ocean–Atmosphere Response Experiment. *Bulletin of the American Meteorological Society*, *73*(9), 1377 - 1416. doi: 10.1175/1520-0477(1992)073⟨1377:TCTCOR⟩2.0.CO;2

Wheeler, M., & Kiladis, G. (1999). Convectively-coupled equatorial waves: Analysis of clouds in the wavenumber-frequency domain. *J. Atmos. Sci.*, *56*, 374–399.

Yanai, M., & Johnson, R. (1993). Impacts of Cumulus Convection on Thermodynamic Fields. In: Emanuel K.A., Raymond D.J. (eds) The Representation of Cumulus Convection in Numerical Models. *Meteorological Monographs*, 39-62. doi: https://doi.org/10.1007/978-1-935704-13-3_4

Yoneyama, K., Zhang, C., & Long, C. N. (2013). Tracking Pulses of the Madden–Julian Oscillation. *Bulletin of the American Meteorological Society*, *94*(12), 1871 - 1891. doi: 10.1175/BAMS-D-12-00157.1

Zhang, C. (2005). Madden-Julian Oscillation. *Rev. Geophys.*, *43*, 1–36.

Zhang, C., Adames, Á. F., Khouider, B., Wang, B., & Yang, D. (2020). Four Theories of the Madden-Julian Oscillation. *Reviews of Geophysics*, *58*(3), e2019RG000685. doi: https://doi.org/10.1029/2019RG000685

Zhang, C., & Hendon, H. H. (1997). Propagating and standing components of the intraseasonal oscillation in tropical convection. *J. Atmos. Sci.*, *54*, 741–752.

Zhang, C., & Ling, J. (2017). Barrier effect of the indo-pacific maritime continent on the mjo: Perspectives from tracking mjo precipitation. *Journal of Climate*, *30*(9), 3439–3459.